ST-11: a new brain-penetrant microtubule-destabilizing agent with therapeutic potential for glioblastoma multiforme

Allison E. Cherry[1], Brian R. Haas[1,*], Alipi V. Naydenov[1,2,*], Susan Fung[1,2], Cong Xu[1], Katie Swinney[1], Michael Wagenbach[3], Jennifer Freeling[4], David A. Canton[1,5], Jonathan Coy[1], Eric A. Horne[1], Barry Rickman[6], Juan Jesus Vicente[3], John D. Scott[1,5], Rodney J. Y. Ho[4], Denny Liggitt[6], Linda Wordeman[3], and Nephi Stella[1,7]

[1]Department of Pharmacology, [2]Graduate Program in Neurobiology & Behavior, [3]Department of Physiology & Biophysics, [4]Department of Pharmaceutics, [5]Howard Hughes Medical Institute, [6]Department of Comparative Medicine, [7]Department of Psychiatry & Behavioral Sciences, University of Washington, 1959 Pacific St., Seattle, WA, 98195

*Authors contributed equally to this paper

Conflict of interest statement: Authors disclose no conflict of interest.

Running title: *ST-11 is a brain-penetrant antitubulin agent that kills GBM*

Keywords: Glioma; Microtubule; Mitosis; Apoptosis; Blood-brain barrier

Financial Support: This work was supported by NIH grants: DA0144861 (N. Stella), GM069429 (L. Wordeman), DA035018 (B.R. Haas), DK54441 (J.D. Scott) and UM1AI120176 (R. J. Y. Ho & J. Freeling).

Correspondence to: Nephi Stella, Department of Pharmacology, Psychiatry & Behavioral Sciences, University of Washington School of Medicine, Box 357290, Seattle, WA, 98195. Tel: (206)-221-5220; Fax: (206)-543-9520; Email: nstella@uw.edu

Abbreviations: AI, alkylindole; GBM, glioblastoma multiforme; i.p., intraperitoneal; LC-MS, liquid chromatography-mass spectrometry; MTD, maximal tolerated dose, MT, microtubule; PARP, poly ADP ribose polymerase; PK, pharmacokinetics.

Word count: 6,060; **Figures:** 6; **Tables:** 1

ABSTRACT (156)

Glioblastoma multiforme (GBM) is a devastating and intractable type of cancer. Current antineoplastic drugs do not improve the median survival of patients diagnosed with GBM beyond 14-15 months in part because the blood-brain barrier is generally impermeable to many therapeutic agents. Drugs that target microtubules (MT) have shown remarkable efficacy in a variety of cancers, yet their use as GBM treatments has also been hindered by the scarcity of brain-penetrant MT-targeting compounds. We have discovered a new alkylindole compound, ST-11, that acts directly on MTs and rapidly attenuates their rate of assembly. Accordingly, ST-11 arrests GBM cells in prometaphase and triggers apoptosis. *In vivo* analyses reveal that unlike current antitubulin agents, ST-11 readily crosses the blood-brain barrier. Further investigation in a syngeneic orthotopic mouse model of GBM shows that ST-11 activates caspase-3 in tumors to reduce tumor volume without overt toxicity. Thus, ST-11 represents the first member of a new class of brain-penetrant antitubulin therapeutic agents.

INTRODUCTION

Gliomas comprise 80% of primary tumors in the central nervous system (1) and the most common subtype is glioblastoma multiforme (GBM, WHO grade IV astrocytoma). Patients diagnosed with GBM have a median overall survival of 14-15 months when treated with a standard regimen of surgery, radiation and the DNA intercalating agent temozolomide (Temodar®) (2). Non-selective chemotherapeutics remain the sole drug treatment option for this patient population in large part because recent targeted therapies, such as gefitinib and bevacizumab that block EGFR and VEGF signaling, respectively, have fallen short of expectations (3-6). This realization has fueled a need for novel therapeutics to combat GBM

through a different mechanism of action; however, the development of new GBM therapeutics is complicated by the necessity for efficient brain penetrance.

A recent study demonstrated that GBM cells are particularly sensitive to mitotic disruption when compared with matched nonmalignant cells (7). This has led to the notion that therapies that perturb microtubule (MT) assembly may represent a promising strategy to manage this type of cancer. For example, recently approved antimitotic devices that generate electromagnetic fields known as tumor treatment fields (TTFields) and function by disrupting MTs show significant efficacy as novel GBM treatments (8, 9). This result indicates that antitubulin agents are likely to show antineoplastic efficacy in patients diagnosed with GBM; however, the majority of antitubulin agents do not readily cross the blood-brain barrier [Reviewed in (10)]. In fact, of the few brain-penetrant antitubulin agents, only 2, sagopilone (ZK-EPO) and the non-analgesic opioid noscapine, have been evaluated for glioma indications (11, 12). However, sagopilone suffered from a lack of efficacy in clinical trials (13), and noscapine required high doses to elicit an effect (12). Irrespective of the limited success of currently available compounds, the susceptibility of GBM cells to mitotic perturbation holds considerable promise for the treatment of this type of cancer (7). To this end, it is necessary to discover and develop novel brain-penetrant antitubulin agents with high therapeutic potential.

Our lab has recently developed a library of alkylindole (AI) compounds with the capacity to kill glioma cells *in vitro* (14, 15). These compounds belong to the broader group of 2-aroylindole agents that inhibit tubulin polymerization by interacting with the colchicine binding site and are insensitive to multidrug resistance efflux pumps that can hinder brain penetrance (16-18). Here, we used a combination of biochemical and cell biology approaches to demonstrate that the AI compound ST-11 arrests the cell cycle and kills glioma cells by directly acting on MTs. To determine the pharmacokinetics (PK) and *in vivo* efficacy of ST-11, we established a stable formulation of this compound in liposomes and developed a liquid

chromatography-mass spectrometry (LC-MS) method to quantify ST-11 in blood and brain. Using these tools, we determined that ST-11 readily penetrates mouse brain after intraperitoneal (i.p.) injection and dose-dependently reduces tumor volume in a syngeneic GBM mouse model. Importantly, ST-11 does not produce overt toxicity in mice. Our study highlights the therapeutic potential of AI compounds as brain-penetrant antitubulin agents with antineoplastic activity in GBM.

MATERIALS & METHODS

See supplement for detailed methods

Chemicals

All chemicals and drugs were purchased from Sigma (St. Louis, MO) unless otherwise noted. JWH-015, and JWH-200 were from Cayman Chemical (Ann Arbor, MI). JWH-120, JWH-148, and JWH-042 were a kind gift from John W. Huffman (Clemson University, Clemson, SC). ST compounds were synthesized in house as described(14, 15). Z-DEVD-FMK was from Santa Cruz Biotechnology (Santa Cruz, CA). L-α-Phosphatidylcholine (EPC) was from Avanti Polar Lipids (Alabastar, AL). 1,2-Dimyristoyl-*sn*-glycero-3-phosphoglycerol, sodium salt (DMPG) and N-(Carbonyl-methosypolyethyleneglycol-2000)-1,2-dimyristoyl-*sn*-glycero-3-phosphoethanolzmine, sodium salt (DMPE-mPEG2000) were from Corden Pharma (Plankstadt, Germany). Cell culture materials were purchased from Life Technologies (Thermo Fisher Scientific, Waltham, MA).

Cell culture

Cells were cultured in DMEM or RPMI containing 10% FBS, 100 U/mL penicillin, and 100 µg/mL streptomycin at 37°C in a 5% CO_2 humidified atmosphere. DBT, T98G, U251, A172, and U87MG cells (ATCC, Manassas, VA) were authenticated by ATCC when purchased using

human short tandem repeat analysis and maintained in culture for less than 6 months. BT74, MGG4 and MGG8 cells were a generous gift from Samuel Rabkin and Hiroaki Wakimoto (Massachusetts General Hospital and Harvard University, Boston, MA) and maintained as floating spheroid cultures in Neurobasal-A medium (19). All spheroid cultures were maintained in *ex vivo* culture for less than 6 months and not authenticated [BT74 as GBM6 in (20), MGG8/8 in (19)]. Primary mouse neuron and astrocyte cultures were prepared as described (21, 22) in accordance with the Institutional Animal Care and Use Committee of the University of Washington.

Viability and proliferation

[^{3}H]-thymidine (5 μCi/ml, Perkin-Elmer, Waltham, MA) was added to cells 30 min after drug treatments and measured at the indicated times by adding 1M NaOH and quantifying radioactivity. WST-1 (Roche, Pleasanton, CA) was used to evaluate cell viability and was measured according to the manufacturer's protocol. For proliferation and cell death using trypan blue exclusion, cells were trypsinized and counted in the presence of trypan blue (1:10, Sigma).

Lysates and western blotting

Western blotting was performed as described previously (23) with the following primary antibodies: cleaved poly ADP ribose polymerase (1:1000, Asp214), cyclin B1 (1:1000, Val152), phospho-histone H3 (1:1000, Ser10), β-tubulin (1:1000), and activated caspase-3 (1:500) were all from Cell Signaling Technologies (Danvers, MA, USA); GAPDH (1:1000) was from Sigma.

MT assembly

MTs were polymerized and sheared in BRB80 (80 mM PIPES-KOH pH 6.85, 1 mM $MgCl_2$, 1 mM EGTA) supplemented with 4% DMSO, 2 mM GTP, 1 mM DTT, 2.5 mM $MgCl_2$ and 60 μM

bovine brain tubulin and added to paclitaxel (Taxol®), nocodazole, or ST-11 to a 1% final DMSO concentration. Details can be found in the *Supplemental methods*. Free tubulin from supernatants and pellets was separated on 4-12% polyacrylamide gels (Thermo-Fisher Scientific, Waltham, MA) and stained with Coomassie G-250. Peak intensities were quantified using ImageJ. Tubulin was purified in-house (24).

Live cell imaging

Cells were transfected with EB3-GFP and RFP-CenpB to label assembling MTs and centromeres, respectively (25). Movies of MT assembly were collected over 30 sec at 500 ms intervals 10 min after drug application (0.5 μM ST-11, 3 μM ST-11, or 1 μM nocodazole) on a Deltavision microscope system (Applied Precision, Issaquah, WA). Images were deconvolved using SoftWorx 5.0 (Applied Precision). MT assembly rates were scored in interphase cells using Fiji TrackMate (26).

Immunocytochemistry

Cells were treated with ST-11 as indicated. Activated caspase-3, MTs, and centromeres were visualized using anti-activated caspase-3 (1:200, Abcam, Cambridge, MA), anti-DM1 alpha (1:500, Sigma), and human anti-centromere (1:100, ACA, Antibodies Inc., Davis, CA) primary antibodies, respectively. Representative images are presented as flat Z-projections (using ImageJ). Spindle profiles and multipolar spindles were scored by hand using a Nikon FX-A microscope (Tokyo, Japan).

Flow cytometry analysis

Cells were lysed in a DAPI-containing lysis solution (146 mM NaCl, 10 mM Tris-base pH 7.4, 2 mM $CaCl_2$, 22 mM $MgCl_2$, 0.05% BSA, 0.1% nonidet P-40, 10 μg/ml DAPI, 10% DMSO) or stained for PI and Annexin V using the Alexa Fluor® 488 Annexin V/Dead Cell Apoptosis Kit

(Thermo Fisher Scientific) according to the manufacturer's protocol. 10,000 events were counted for each condition using an LSRII flow cytometer (BD Biosciences). Data were analyzed using FCS Express (v4 De Novo Software, Glendale, CA) equipped with the MultiCycle plugin. See *Supplemental methods* for details.

ST-11 nanoparticle formulation

The chemical parameters of ST-11 were determined using Chemicalize Beta (www.chemicalize.org). The likelihood of ST-11 brain penetration was estimated using the induction tree models outlined by (27). EPC:DMPG:DMPE-mPEG2000 (9:1:0.5 m/m/m) nanoparticles containing ST-11 for *in vivo* studies were produced as described previously (28). Details can be found in the *Supplemental methods*.

Pilot safety studies

All animal experiments were conducted in accordance with the American Association for Accreditation of Laboratory Animal Care, and all procedures were approved by the University of Washington Institutional Animal Care and Use Committee. A 5-day dose-range finding study was performed following screening for maximum tolerated dose. CD1 mice received once daily intraperitoneal (i.p.) dosing with 15, 40, 80, 160 or 240 mg/kg ST-11, or the corresponding volume of liposome vehicle. Mice were monitored for signs of general distress, including ataxia, squinting, piloerection, hunching, bradykinesia and dyspnea. Additionally, mice were monitored for organ dysfunction and/or moribund state. Mice were then euthanized and organs were harvested for histopathological analysis by a board-certified veterinary pathologist (Dr. Denny Liggitt) who was blinded to group assignment.

Tissue extraction and ST-11 quantification by LC-MS

Lipids were isolated from CD1 mouse blood and whole brain, and JWH-015 was used as an internal standard for quantification. Lipid composition was analyzed using a Waters Micromass

Quattro Premier XE (Milford, MA) equipped with a C18 LC column (AQUITY UPLC BEH C18 1.7 µm 2.1×100mm, Waters, Munich, Germany). Compounds were distinguished by their ES+ daughter ions with ST-11 at 169 m/z and JWH-015 at 155 m/z. ST-11 was quantified using a ratio of the area under the curve (AUC) of ST-11/AUC of JWH-015 and extrapolating from the linear standard curve. Details can be found in *Supplemental methods*.

Orthotopic DBT tumors and treatment regimen

2×10^4 DBT cells were implanted in 8 week-old mail BALB-c mice at 2 mm cranial from bregma and 1.5 mm left lateral. Details can be found in *Supplemental methods*. Tumors exhibited features of aggressive progression within 3 weeks, including frequent mitotic figures, multifocal necrosis, edema, and densely arranged neoplastic cells with enhanced cellular atypia, anisocytosis and anisokaryosis (Figure S1). Mice were distributed into 4 arms 1 week after implantation: vehicle (liposome-only), 5 mg/kg, 15 mg/kg and 40 mg/kg ST-11, and they received daily i.p. injections for 2 weeks. Mice were euthanized and perfused with 4% paraformaldehyde, and whole brains were harvested.

H&E and Immunohistochemistry (IHC)

Whole brains were stained as described previously (29), with the following primary antibodies: anti-activated caspase-3 (1:200, Abcam) and anti-Iba-1 (1:1000, Abcam). For H&E staining, fixed brains were either sent to Histology Consultation Services (Everson, WA), or processed in-house using a standard method (5 sec in concentrated Mayer's hematoxylin and 60 sec in concentrated Eosin Y).

Tumor volume

Tumor volume was estimated by slab approximation (30). Details can be found in *Supplemental methods*. Large numbers of microglia invade GBM tumor masses [Reviewed in (31)] (Figure S2). We calculated the percentage of infiltrating microglia in each tumor using semi-

quantitative IHC as described previously (29) and subtracted this value from the calculated tumor volume to obtain the adjusted tumor volume.

Statistical Analysis

GraphPad Prism (v5.01, La Jolla, CA) was used for statistical analysis. Data are presented as the mean ± SEM, and statistical significance was determined using Student's t-test, a one-way ANOVA followed by a Dunnett's or Tukey *post-hoc* test, or a two-way ANOVA followed by a Bonferroni *post-hoc* test.

RESULTS

ST-11 inhibits proliferation and kills GBM cells in vitro

A library of 10 AI analogues was screened for activity on the human GBM cell line T98G (Table S1). One compound, named ST-11, exhibited a combination of properties requisite for further mechanistic and *in vivo* analyses: it reduced T98G cell number with the highest potency and efficacy, and it encompasses the basic chemical scaffold of the series (colloquially termed the ST compound library) (Figure 1A, Table S1). Thus, ST-11 was selected for further screening on additional human GBM cell lines, including 3 adherent cell lines (U251, A172 and U87MG cells) and 3 stem cell lines (BT74, MGG4 and MGG8) (32). ST-11 reduced cell number in all of the GBM lines tested when applied at micromolar concentrations (EC_{50} from 2.4 – 8.6 μM, maximal efficacy from 51 – 96%) (Table 1). A vital and desired feature of any new antineoplastic drug is a favorable therapeutic index, which is related to the preferential activity of the compound for tumor cells. Thus, we tested the antineoplastic activity of ST-11 on malignant and non-malignant mouse cells. ST-11 killed mouse DBT glioma cells with a potency and efficacy similar to T98G cells (EC_{50} = 2.5 μM, maximal efficacy = 60.7%). Notably, this compound did not affect the viability of primary mouse astrocytes or neurons (Figure 1B). Therefore, ST-11

preferentially targets a variety of GBM cell lines, including glioma stem cells, which tend to be refractive to therapy (33, 34).

A loss of cell number can result from reductions in cell proliferation and/or increases in cell death. In order to delineate between both outcomes, we initially determined if ST-11 reduces cell viability using a trypan blue exclusion assay. ST-11 dose-dependently increased the percentage of trypan blue-positive dead cells with a potency and efficacy similar to what was detected using WST-1 (WST-1 EC_{50} = 2.5 μM, maximal efficacy = 66%; trypan blue EC_{50} = 4.3 μM, maximal efficacy = 68%, WST-1 EC_{50} = 2.5 μM, maximal efficacy = 66%) (Table S1, Figure 1C). We ascertained that ST-11 reduces cell proliferation using 2 independent approaches. First, we measured the dose-dependent effects of ST-11 on [^{3}H]-thymidine incorporation in T98G and DBT cells and found that this compound reduced [^{3}H]-thymidine incorporation in both T98G and DBT cells within 24 hrs of treatment (Figure 1D and S3A). Second, we monitored the time-dependent effects of ST-11 action on the accumulation of 2 mitotic markers: cyclin-B1 and phospho-histone H3. Application of ST-11 led to an increase in both cyclin-B1 and phospho-histone H3 levels (Figure 1E and 1F). Thus, we propose that ST-11 reduces GBM cell number by arresting cells in mitosis and subsequently killing them.

ST-11 arrests cells in prometaphase by directly targeting MTs

To further confirm our hypothesis that ST-11 arrests GBM cells in mitosis, we used flow cytometry to analyze the proportion of cells in each cell cycle phase. Treatment with ST-11 increased the percentage of T98G and DBT cells in G2/M phase and decreased the number of cells in G1 phase (Figure 2A and S3B). To determine whether this effect resulted from cell cycle arrest in mitosis, we quantified the proportion of cells in each stage of mitosis after application of ST-11. Our compound increased the percentage of prometaphase T98G and DBT cells in a dose-dependent manner (Figure 2B and S3C), suggesting that ST-11 arrests cells in mitosis by

triggering the spindle assembly checkpoint [reviewed in (35, 36)]. In line with this observation, we also noted that ST-11 both dose-dependently increased the proportion of cells with multipolar spindles (Figure 2C and S3D) and induced severe defects in chromosomal biorientation (Figure 2D).

Improper spindle assembly can be attributed to defects in MT dynamics and polymerization, and 2-aroylindole agents are known to directly depolymerize MTs (16, 17, 37, 38). Therefore, we used 3 approaches to determine whether ST-11 was acting directly on MTs. First, we used a cell-free assay with purified tubulin to assess the partitioning of MT dimers and polymer. As expected, the MT destabilizing agent nocodazole triggered an increase the free tubulin (Figure 3A). Conversely, a decrease in free tubulin levels was observed upon addition of the MT stabilizing agent paclitaxel (Figure 3A). Similar to nocodazole, ST-11 dose-dependently increased the level of free tubulin, which corresponds to MT disassembly (Figure 3A). Thus, ST-11 destabilizes MTs in a cell-free system containing purified MTs, implying that it directly acts on tubulin. The EC_{50} of ST-11 on MT destabilization (EC_{50} = 3.7 μM) is similar to its EC_{50} on T98G and DBT cell viability, indicating MTs may be the direct molecular target of ST-11 involved in its antineoplastic effect. Second, we assessed whether ST-11 affected MT polymer levels in T98G cells *in vitro*. MTs were significantly less abundant in T98G cells treated with ST-11, demonstrating that this compound directly acts on MTs in cells (Figure 3B). Lastly, using live cell imaging of EB3-GFP on assembling MTs in T98G cells, we found that sub-micromolar concentrations of ST-11 (0.5 μM) decreased the MT assembly rate by 32% within 10 min of treatment (Figure 3C and 3D, Movies S1 and S2). Importantly, the effects of ST-11 on MT assembly were reversible by 24 hrs after drug removal (Figure S4A). Nocodazole and ST-11 both exhibit robust MT depolymerizing activity on purified tubulin (Figure 3A). To compare the activity of these compounds on live T98G cells, we selected concentrations of ST-11 (3 μM) and nocodazole (1 μM) that exhibit comparable MT destabilizing activity on purified tubulin

(Figure 3A). We noted that nocodazole abolished all assembling MTs in live T98G cells by 15 min (Figure S4B). In contrast, MTs continued to assemble after ST-11 treatment (3 μM) (Figure S4B) albeit more slowly. Thus, while ST-11 has a significant effect on cell cycle arrest at this concentration (Figure 2B), it does not abolish all dynamic MTs in interphase cells compared with nocodazole. Together, these results demonstrate that ST-11 directly acts on MTs to reduce MT assembly, leading to mitotic spindle defects and prometaphase arrest in GBM cells.

ST-11 activates caspase-3-dependent apoptosis

Antitubulin agents often promote caspase-dependent apoptosis (39). Therefore, we sought to determine whether ST-11 activated apoptosis in GBM cells *in vitro*. ST-11 induced caspase-3 activation in both T98G and DBT cells as early as 2-6 hrs after treatment (Figure 4A and S3E). This result was confirmed by western blot analysis 24 hrs after treatment with ST-11 (Figure 4B). Accordingly, this compound induced time-dependent cleavage of poly ADP ribose polymerase (PARP) (Figure 4C). Moreover, cells exhibited nuclear condensation and membrane blebbing within 24 and 48 hrs of ST-11 treatment, respectively (Figure 4A). Control experiments confirmed that inhibition of caspase-3 with Z-DEVD-FMK blocked the antineoplastic action of ST-11 (Figure 4D). ST-11 treatment for 24 hrs increased both propidium iodide (PI) and Annexin V staining quantified with flow cytometry (Figure S5). Therefore, ST-11 activates caspase-3-dependent apoptosis in GBM cells.

To compare the *in vitro* efficacy of ST-11 with other antitubulin agents, we measured the time-dependent effects of ST-11, paclitaxel and nocodazole on T98G cell number using WST-1. By 12 hrs, all 3 compounds had reduced cell number by 10–15%. However, by 72 hrs, paclitaxel was inactive, whereas cell number was reduced by 34% with nocodazole and by 48% with ST-11 (Figure 4E). Notably, paclitaxel is known to have reduced activity in T98G cells due to their high expression of multidrug resistance (MDR) efflux pumps, such as MDR-1 (40).

In contrast, paclitaxel reduced the viability of MDA-MB-231 breast cancer cells used as a positive control by 72 hrs (Figure S6). This finding underscores the ability of ST-11 to retain efficacy in a cell line that expresses high levels of MDR pumps, a feature maintained by other 2-aroylindole compounds (17, 41). ST-11 was therefore more effective at reducing cell number than 2 antitubulin compounds, one of which (paclitaxel) is widely used in the clinic as an antineoplastic drug. These findings suggest that further research into the *in vivo* safety and efficacy of ST-11 is warranted.

Solubility and safety of ST-11 in vivo

Because ST-11 does not adversely affect the viability non-malignant cells *in vitro*, we sought to study its safety and efficacy *in vivo.* We first assessed the maximal tolerated dose (MTD) and pharmacokinetic profile of ST-11 in healthy mice. The lipophilic nature of ST-11 necessitated the development of a stable formulation of this compound. Standard solvents such as 30% mouse serum, 10% ethanol, 1% DMSO, 1% Tween-80, 2% Tween-80, 1:1:18 ethanol:Cremophor® RH40:saline, or 1% Tween-80 + 10% FBS did not solubilize ST-11 (Figure S7). Thus, we explored liposome formulations, which are composed of combinations of lipids that form semi-solid nanospheres (42). Our analyses revealed that ST-11 was soluble and stable for at least 14 days in nanospheres composed of 9:1:0.5 (m/m/m) EPC:DMPG:DMPE-mPEG2000 at a final lipid-to-drug ratio of 6:1 (m/m) (experimental details in *Materials & methods* and *Supplemental methods*). This formulation was used to administer ST-11 in all subsequent *in vivo* experiments.

Initially, we assessed the MTD of ST-11 in a 5-day pilot dose-range finding study. Mice were treated with ST-11 (15, 40, 80, 160, and 240 mg/kg, i.p.) and monitored for signs of distress (see *Materials & methods*). No adverse effects were observed when the compound was administered at doses up to 240 mg/kg daily over 5 days, indicating that ST-11 appears to

be well tolerated. Additionally, tissue damage was assessed using H&E staining of 6 principal organs (heart, liver, kidney, lungs, spleen and brain). No signs of tissue injury were observed in any organ harvested from any ST-11 dosage group. However, we noted a prominence of slightly foamy macrophages in the marginal zone of the spleen of mice treated with both 240 mg/kg ST-11 and the matched liposome-only control. This finding indicates that the large amount of liposomes injected in this condition induced a high rate of liposome phagocytosis in a manner that was independent of ST-11 (data not shown). This pilot safety study indicates that ST-11 is well tolerated at high doses and does not produce overt toxic effects when administered daily over a wide dose range.

Pharmacokinetic profile of ST-11

A limiting factor of the use of many antitubulin agents to treat GBM is their inability to cross the blood-brain barrier [Reviewed in (10)]. Therefore, we used predictive models to determine the likelihood that ST-11 is brain-penetrant. Based on 2 decision tree induction models described in (27), ST-11 is predicted to cross the blood-brain barrier (LogP = 5.81, rotatable bonds = 3, and polar surface area = 22). To confirm our predictions, we established the PK profile of ST-11 in healthy mice to evaluate whether this compound reaches the brain at concentrations that could produce antineoplastic activity (*i.e.* above its EC_{50} for killing GBM cells in culture). We developed an LC-MS method to quantify ST-11 in biological matrices using a related compound, JWH-015, as an internal standard (see chemical structure in Table S1). Both compounds eluted at ~2.8 min (Figure 5A) and were independently detected with base peaks of 169.0 (ST-11) and 155.0 m/z (JWH-015) (Figure 5B and 5C). The quantification of ST-11 was linear from 30 fg to 1 ng (r^2>0.99) upon analyzing the compound when spiked into either blood or brain matrices (Figure 5D). The limit of detection was 100 fg and the limit of quantitation was

3 pg (error <10%). Thus, our newly developed method allows for the reliable and precise quantification of ST-11 from 0.1 to 1 ng in samples from mouse blood serum and brain tissue.

To establish the PK profile of ST-11, mice were treated with ST-11 (40 mg/kg, i.p.), and blood and brain tissue were harvested 10, 30, 60, 90, and 480 min after injections. Serum levels of ST-11 peaked after 10 min (C_{max} = 15.3 ± 3.6 μM), declined steadily thereafter and reached undetectable levels within 8 hrs post-injection (Figure 5E). By contrast, brain levels of ST-11 peaked after 60 min (C_{max} = 8.7 ± 0.9 μM) and remained above its average antineoplastic EC_{50} (*i.e.* 1.8 ± 0.2 μM) for up to 8 hrs. In a follow-up experiment, mice were treated with 5, 15, or 40 mg/kg ST-11 (i.p.), and blood and brain tissue were harvested 60 min post-injection. Both 15 and 40 mg/kg injections led to brain levels of ST-11 that were greater than the EC_{50} for killing GBM cells (Figure 5F). Hence, liposomes deliver micromolar concentrations of ST-11 to the brain within 60 min of i.p. injection that remain above its efficacious concentration for killing GBM cells for 4–8 hrs.

ST-11 induces apoptosis in orthotopic DBT tumors and reduces tumor volume

Finally, to determine if ST-11 affects GBM growth *in vivo*, we used a syngeneic mouse model in which DBT cells were orthotopically implanted into BALB/c mice (Figure 6A, S1 and S2). One week after DBT cell implantation, mice were treated daily with 5, 15 or 40 mg/kg ST-11 or the corresponding liposome vehicle for 2 weeks. The total volume of each tumor after 2 weeks was estimated by slab approximation and adjusted for the abundant invasion of microglia using semi-quantitative IHC analysis of Iba-1 (Figure S2). ST-11 treatment promoted a dose-dependent reduction in tumor volume (Figure 6B). Importantly, we detected a dose-dependent increase in caspase-3 activation, nuclear condensation and cellular loss within the tumor mass (Figure 6C). Collectively, these results indicate that i.p. administration of ST-11 dose-

dependently activates apoptosis and reduces the volume of orthotopically implanted DBT tumors.

DISCUSSION

In this study, we describe the pharmacology and mechanism of action of ST-11, a new AI compound that destabilizes MTs. This compound displays 3 properties that are requisite for treating GBMs: 1) the ability to cross the blood-brain barrier, 2) preferential selectivity for killing GBM cells and 3) a favorable safety profile when administered at doses above its therapeutic efficacy. Our study not only provides a solid foundation for further chemical optimization of this compound but also launches the pharmacological and biological characterization of this new class of brain-penetrant antitubulin agents. Accordingly, ST-11 and future derivatives may prove to be efficacious for the treatment of brain cancers such as GBM, which remain both one of the most devastating and therapeutically intractable forms of cancer.

ST-11 reduces GBM cell number by reducing both proliferation and viability. Mechanistically, we have discovered that, similar to other 2-aroylindoles, this compound acts directly on MTs to reduce their assembly. The EC_{50}s of the effects of ST-11 on MT destabilization in a cell-free assay and GBM cell viability are comparable. Taken together, these findings infer that tubulin is likely the primary target of this compound. Consistent with this result, ST-11 reduced the level of MT polymer and, at lower concentrations, the rate of assembling MTs. In living cells, MTs rapidly interconvert between assembly and disassembly. This dynamic action is essential for the proper spindle assembly, chromosome attachment and segregation during mitosis (43). Accordingly, we concluded that ST-11 suppressed MT dynamics in a manner that leads to aberrant spindle formation, improper alignment of chromosomes and cell cycle arrest in a prometaphase-like configuration. This effect is

consistent with mitotic checkpoint arrest produced by the MT destabilizing activity of this compound.

Several important features distinguish ST-11 from nocodazole, which, similarly to 2-aroylindoles, directly interacts with the colchicine binding site. ST-11 and nocodazole exhibit different effects on MT dynamics in live T98G cells at concentrations that promote similar levels of MT depolymerization in a cell-free system. Nocodazole rapidly abolishes dynamic MTs whereas ST-11 leaves them intact. Like nocodazole, the effects of ST-11 on suppression of MT dynamics are fully reversible within 24 hrs. These findings are significant for 2 reasons. First, the reversibility of this compound might limit toxicity, which is notable from a therapeutic standpoint. Irreversible MT destabilizing compounds, such as colchicine, often have a challenging therapeutic index and their clinical use can be hindered by toxicity (36). Second, while ST-11 potently arrests cells in mitosis, its effects on interphase MT dynamics appear to be less severe. Likewise, this property may limit the clinical toxicity of this compound toward non-dividing cells, especially neuronal cells.

Drugs that disrupt MT dynamics are commonly prescribed therapeutics as they both reduce tumor cell proliferation and trigger apoptosis (36, 39). Our finding that ST-11 kills GBM cells through the activation of caspase-3-dependent apoptosis is evidenced by caspase-3 and PARP cleavage, morphological changes, and increases in Annexin V/PI staining. Further support for this postulate is provided from our investigation of ST-11 on T98G cells where induction of apoptosis was ablated upon pretreatment with the caspase-3 inhibitor Z-DEVD-FMK. Therefore, we conclude that the principle mechanism of action of ST-11 is to directly suppress MT assembly, which leads to defects in mitotic spindle formation and chromosome attachment. This response is known to trigger mitotic checkpoint arrest and ultimately render glioma cells susceptible to apoptotic cell death [reviewed in (36)].

A recent study designed to identify novel therapeutic targets for the treatment of GBM that do not adversely affect healthy brain cells revealed that this type of cancer is particularly sensitive to mitotic disruption (7). Other investigators have examined the efficacy and potency of indole-containing compounds on MT disruption and tumor reduction using different cancer models (16, 17, 37). For example, the antitubulin agent BPR0L075 effectively reduces tumor size in flank xenograft models of gastric and cervical carcinomas (17). Importantly, our studies suggest that ST-11 has increased therapeutic potential over other classical antitubulin compounds. Specifically, it has a higher efficacy and more lasting effect than either paclitaxel or nocodazole on the viability of GBM cells *in vitro.* Thus, as a novel brain-penetrant compound, ST-11 underscores the therapeutic potential of antitubulin agents for the treatment of GBM.

Another feature of our study was the establishment of ST-11 brain permeability. We observed that single injections of 15 and 40 mg/kg resulted in micromolar concentrations of ST-11 in brain that exceed its EC_{50} for killing GBM cells in culture for 4-8 hours. Additionally, the brain concentration of ST-11 was higher than that found in plasma by 2 hours post-administration with a brain:serum ratio of 1.2. Importantly, while possible and limited, liposomes are not known to favor passage across the blood-brain barrier without the aid of other factors such as convection-enhanced delivery (CED) (44), ultrasound focused ultrasound (45) or receptor mediated processes. Accordingly, it is likely that ability of formulated ST-11 to permeate the brain and provide significant efficacy against orthotopic gliomas represents an intrinsic property of ST-11. The structure-based predictions suggesting the brain-penetrating qualities of ST-11 provide additional support to this possibility. Hence, ST-11 dose-dependently activated caspase-3 and reduced intracranial tumor volume when delivered i.p. daily for 2 weeks. Notably, we did not observe overt signs of toxicity in these mice during the treatment period (data not shown). Moreover, we monitored the MTD of ST-11 in a 5-day dose-

range finding study that incorporated clinical and histopathologic assessments. These rudimentary analyses of ST-11 toxicity indicate that this compound does not produce overt side effects when administered chronically at 40 mg/kg or acutely up to 240 mg/kg *in vivo*. This result agrees with our *in vitro* finding that ST-11 is nontoxic to non-malignant cells. Thus, we have derived a new delivery method that achieves therapeutic brain-levels of ST-11 and exhibits an encouraging safety profile when assessed in mice.

To conclude, our study introduces ST-11 as a new brain-penetrant antineoplastic agent with preferential selectivity for GBM cells and no discernible toxicities in mice. The use of antitubulin agents for the treatment of GBM is all the more convincing when one considers that they act in a manner that has been anticipated to be effective for the treatment of this type of cancer (7). We therefore propose that ST-11 belongs to a promising new series of brain-penetrant antineoplastic agents that slow MT assembly, promote cell cycle arrest and trigger apoptosis in GBM. The future development and characterization of ST-11 analogs may ultimately lead to the advent of a treatment of this intractable and debilitating form of brain cancer.

Acknowledgements

We would like to acknowledge the following individuals for their contributions to this study: Dr. Robert Rostomily at the University of Washington (Seattle, WA) for years of helpful discussions; Dr. Anna Akhmanova at Utrecht University (Utrecht, The Netherlands) for providing EB3-GFP, Dale Whittington at the School of Pharmacy's Mass Spectrometry Center at University of Washington (Seattle, WA) for assisting with the development of the LC-MS technique and use of the core facility; Drs. Samuel Rabkin and Hiroaki Wakimoto at the Massachusetts General Hospital and Harvard Medical School (Boston MA) for providing MGG4 and MGG8; Donna Prunkard at the University of Washington (Seattle, WA) for assisting in the collection and

analysis of flow cytometry data; and Glen MacDonald at the University of Washington (Seattle, WA) for assisting with confocal image collection and analysis.

References

1. Ostrom QT, Gittleman H, Liao P, Rouse C, Chen Y, Dowling J, et al. CBTRUS statistical report: Primary brain and central nervous system tumors diagnosed in the united states in 2007-2011. Neuro Oncol 2014;16 Suppl 4:iv1-63.

2. Stupp R, Mason WP, van den Bent MJ, Weller M, Fisher B, Taphoorn MJ, et al. Radiotherapy plus concomitant and adjuvant temozolomide for glioblastoma. N Engl J Med 2005;352:987-96.

3. Rich JN, Reardon DA, Peery T, Dowell JM, Quinn JA, Penne KL, et al. Phase II trial of gefitinib in recurrent glioblastoma. J Clin Oncol 2004;22:133-42.

4. Gilbert MR, Dignam JJ, Armstrong TS, Wefel JS, Blumenthal DT, Vogelbaum MA, et al. A randomized trial of bevacizumab for newly diagnosed glioblastoma. N Engl J Med 2014;370:699-708.

5. de Groot JF, Fuller G, Kumar AJ, Piao Y, Eterovic K, Ji Y, et al. Tumor invasion after treatment of glioblastoma with bevacizumab: Radiographic and pathologic correlation in humans and mice. Neuro Oncol 2010;12:233-42.

6. Keunen O, Johansson M, Oudin A, Sanzey M, Rahim SA, Fack F, et al. Anti-VEGF treatment reduces blood supply and increases tumor cell invasion in glioblastoma. Proc Natl Acad Sci U S A 2011;108:3749-54.

7. Ding Y, Hubert CG, Herman J, Corrin P, Toledo CM, Skutt-Kakaria K, et al. Cancer-specific requirement for BUB1B/BUBR1 in human brain tumor isolates and genetically transformed cells. Cancer Discov 2013;3:198-211.

8. Stupp R, Wong ET, Kanner AA, Steinberg D, Engelhard H, Heidecke V, et al. NovoTTF-100A versus physician's choice chemotherapy in recurrent glioblastoma: A randomised phase III trial of a novel treatment modality. Eur J Cancer 2012;48:2192-202.

9. Kirson ED, Gurvich Z, Schneiderman R, Dekel E, Itzhaki A, Wasserman Y, et al. Disruption of cancer cell replication by alternating electric fields. Cancer Res 2004;64:3288-95.

10. Dumontet C, Jordan MA. Microtubule-binding agents: A dynamic field of cancer therapeutics. Nat Rev Drug Discov 2010;9:790-803.

11. Hoffmann J, Fichtner I, Lemm M, Lienau P, Hess-Stumpp H, Rotgeri A, et al. Sagopilone crosses the blood-brain barrier in vivo to inhibit brain tumor growth and metastases. Neuro Oncol 2009;11:158-66.

12. Landen JW, Hau V, Wang M, Davis T, Ciliax B, Wainer BH, et al. Noscapine crosses the blood-brain barrier and inhibits glioblastoma growth. Clin Cancer Res 2004;10:5187-201.

13. Stupp R, Tosoni A, Bromberg JE, Hau P, Campone M, Gijtenbeek J, et al. Sagopilone (ZK-EPO, ZK 219477) for recurrent glioblastoma. A phase II multicenter trial by the european organisation for research and treatment of cancer (EORTC) brain tumor group. Ann Oncol 2011;22:2144-9.

14. Kline T, Stella N, inventors; University of Washington Through Its Center For Commercialization, assignee. Composition and methods for treating glioblastoma. patent US 13/818,026. 2013 August 1.

15. Kline T, Stella N, inventors; University of Washington Through Its Center For Commercialization, assignee. Composition and methods for treating glioblastoma. patent PCT/US2011/048594. 2012 April 26.

16. Beckers T, Reissmann T, Schmidt M, Burger AM, Fiebig HH, Vanhoefer U, et al. 2-aroylindoles, a novel class of potent, orally active small molecule tubulin inhibitors. Cancer Res 2002;62:3113-9.

17. Kuo CC, Hsieh HP, Pan WY, Chen CP, Liou JP, Lee SJ, et al. BPR0L075, a novel synthetic indole compound with antimitotic activity in human cancer cells, exerts effective antitumoral activity in vivo. Cancer Res 2004;64:4621-8.

18. Loscher W, Potschka H. Blood-brain barrier active efflux transporters: ATP-binding cassette gene family. NeuroRx 2005;2:86-98.

19. Wakimoto H, Kesari S, Farrell CJ, Curry WT,Jr, Zaupa C, Aghi M, et al. Human glioblastoma-derived cancer stem cells: Establishment of invasive glioma models and treatment with oncolytic herpes simplex virus vectors. Cancer Res 2009;69:3472-81.

20. Pandita A, Aldape KD, Zadeh G, Guha A, James CD. Contrasting in vivo and in vitro fates of glioblastoma cell subpopulations with amplified EGFR. Genes Chromosomes Cancer 2004;39:29-36.

21. Saura J, Tusell JM, Serratosa J. High-yield isolation of murine microglia by mild trypsinization. Glia 2003;44:183-9.

22. Marrs WR, Horne EA, Ortega-Gutierrez S, Cisneros JA, Xu C, Lin YH, et al. Dual inhibition of alpha/beta-hydrolase domain 6 and fatty acid amide hydrolase increases endocannabinoid levels in neurons. J Biol Chem 2011;286:28723-8.

23. Canton DA, Keene CD, Swinney K, Langeberg LK, Nguyen V, Pelletier L, et al. Gravin is a transitory effector of polo-like kinase 1 during cell division. Mol Cell 2012;48:547-59.

24. Hyman A, Drechsel D, Kellogg D, Salser S, Sawin K, Steffen P, et al. Preparation of modified tubulins. Methods Enzymol 1991;196:478-85.

25. Wordeman L, Wagenbach M, von Dassow G. MCAK facilitates chromosome movement by promoting kinetochore microtubule turnover. J Cell Biol 2007;179:869-79.

26. Jaqaman K, Loerke D, Mettlen M, Kuwata H, Grinstein S, Schmid SL, et al. Robust single-particle tracking in live-cell time-lapse sequences. Nat Methods 2008;5:695-702.

27. Suenderhauf C, Hammann F, Huwyler J. Computational prediction of blood-brain barrier permeability using decision tree induction. Molecules 2012;17:10429-45.

28. Freeling JP, Koehn J, Shu C, Sun J, Ho RJ. Long-acting three-drug combination anti-HIV nanoparticles enhance drug exposure in primate plasma and cells within lymph nodes and blood. AIDS 2014;28:2625-7.

29. Horne EA, Coy J, Swinney K, Fung S, Cherry AE, Marrs WR, et al. Downregulation of cannabinoid receptor 1 from neuropeptide Y interneurons in the basal ganglia of patients with huntington's disease and mouse models. Eur J Neurosci 2013;37:429-40.

30. Schmidt KF, Ziu M, Schmidt NO, Vaghasia P, Cargioli TG, Doshi S, et al. Volume reconstruction techniques improve the correlation between histological and in vivo tumor volume measurements in mouse models of human gliomas. J Neurooncol 2004;68:207-15.

31. da Fonseca AC, Badie B. Microglia and macrophages in malignant gliomas: Recent discoveries and implications for promising therapies. Clin Dev Immunol 2013;2013:264124.

32. Wakimoto H, Mohapatra G, Kanai R, Curry WT,Jr, Yip S, Nitta M, et al. Maintenance of primary tumor phenotype and genotype in glioblastoma stem cells. Neuro Oncol 2012;14:132-44.

33. Bao S, Wu Q, McLendon RE, Hao Y, Shi Q, Hjelmeland AB, et al. Glioma stem cells promote radioresistance by preferential activation of the DNA damage response. Nature 2006;444:756-60.

34. Liu G, Yuan X, Zeng Z, Tunici P, Ng H, Abdulkadir IR, et al. Analysis of gene expression and chemoresistance of CD133+ cancer stem cells in glioblastoma. Mol Cancer 2006;5:67.

35. Lara-Gonzalez P, Westhorpe FG, Taylor SS. The spindle assembly checkpoint. Curr Biol 2012;22:R966-80.

36. Mollinedo F, Gajate C. Microtubules, microtubule-interfering agents and apoptosis. Apoptosis 2003;8:413-50.

37. Kaufmann D, Pojarova M, Vogel S, Liebl R, Gastpar R, Gross D, et al. Antimitotic activities of 2-phenylindole-3-carbaldehydes in human breast cancer cells. Bioorg Med Chem 2007;15:5122-36.

38. Mahboobi S, Pongratz H, Hufsky H, Hockemeyer J, Frieser M, Lyssenko A, et al. Synthetic 2-aroylindole derivatives as a new class of potent tubulin-inhibitory, antimitotic agents. J Med Chem 2001;44:4535-53.

39. Topham CH, Taylor SS. Mitosis and apoptosis: How is the balance set? Curr Opin Cell Biol 2013;25:780-5.

40. Bahr O, Rieger J, Duffner F, Meyermann R, Weller M, Wick W. P-glycoprotein and multidrug resistance-associated protein mediate specific patterns of multidrug resistance in malignant glioma cell lines, but not in primary glioma cells. Brain Pathol 2003;13:482-94.

41. Lu Y, Chen J, Xiao M, Li W, Miller DD. An overview of tubulin inhibitors that interact with the colchicine binding site. Pharm Res 2012;29:2943-71.

42. Kraft JC, Freeling JP, Wang Z, Ho RJ. Emerging research and clinical development trends of liposome and lipid nanoparticle drug delivery systems. J Pharm Sci 2014;103:29-52.

43. Meunier S, Vernos I. Microtubule assembly during mitosis - from distinct origins to distinct functions? J Cell Sci 2012;125:2805-14.

44. MacKay JA, Deen DF, Szoka FC,Jr. Distribution in brain of liposomes after convection enhanced delivery; modulation by particle charge, particle diameter, and presence of steric coating. Brain Res 2005;1035:139-53.

45. Negishi Y, Yamane M, Kurihara N, Endo-Takahashi Y, Sashida S, Takagi N, et al. Enhancement of blood-brain barrier permeability and delivery of antisense oligonucleotides or plasmid DNA to the brain by the combination of bubble liposomes and high-intensity focused ultrasound. Pharmaceutics 2015;7:344-62.

Tables

Cells	Potency (μM)	Efficacy (% Dead)
MGG8	4.6	96.0
BT74	2.4	89.9
A172	5.8	68.2
U251	4.3	67.0
T98G	2.5	65.7
U87	5.5	63.2
MGG4	8.6	51.3

Table 1: ST-11 kills cultured GBM cells. GBM cell lines were treated with ST-11, and cell number was measured after 72 hrs using WST-1. Dose-response curves were analyzed and data shown are the mean ± SEM from at least 3 independent experiments.

Figure legends

Figure 1: ST-11 reduces proliferation and kills GBM cells

(A) Chemical structure of ST-11. (B) Viability of cultured mouse DBT, astrocytes and neurons measured with WST-1 72 hrs after ST-11 treatment. (C) T98G cell death measured with trypan blue 72 hrs after ST-11 treatment. (D) [^{3}H]-thymidine incorporation in T98G cells 24 hrs after ST-11 treatment. (E-F) The time-dependent accumulation of cyclin-B1 and phospho-histone H3 after ST-11 treatment (3 μM) shown by a representative western blot (E) and quantified

using GAPDH as a loading control (F). Data are the mean ± SEM of at least 3 independent experiments.

Figure 2: ST-11 arrests cultured T98G cells in prometaphase

(A) Cell cycle analysis of T98G cells treated with ST-11 (blue) or vehicle (red) for 24 hrs using flow cytometry. The percentages of cells in G1, S, and G2/M phases are indicated. (B) Percentage of cells in each stage of mitosis after treatment with ST-11. *$p<0.05$, ‡$p<0.001$ compared with vehicle, two-way ANOVA with Bonferroni *post-hoc* test. (C) ST-11 dose-dependently increases the formation of multipolar spindles. **$p<0.01$, ‡$p<0.001$ compared with vehicle, one-way ANOVA with Tukey *post-hoc* test. Data are the mean ± SEM of at least 3 independent experiments. (D) Representative images of ST-11-induced (5 μM) abnormalities in chromosomal alignment (arrowheads). Tubulin is shown in red, centromeres in green, and DNA in blue. Scale bars: 10 μm.

Figure 3: ST-11 directly destabilizes MTs and decreases their assembly in T98G cells

(A) Incubation of ST-11 with purified tubulin induced a dose-dependent increase in free tubulin. Paclitaxel and nocodazole were used as positive controls to decrease and increase free tubulin, respectively. The dashed line indicates the steady-state level of free tubulin established prior to the addition of antitubulin agents (7.8 μM). Results are the mean ± SEM of at least 3 independent experiments. (B) Representative images of ST-11 (5 μM) disrupting MTs in T98G cells. Tubulin is shown in red, centromeres in green, and DNA in blue. Scale bars: 10 μm. (C-D) ST-11 (0.5 μM) slows MT dynamics in live T98G cells within 10 min of treatment (C, quantified in D). *$p<0.05$, Student's t-test. Scale bars: 10 μm. Data are the mean ± SEM of at least 3 independent experiments.

Figure 4: ST-11 triggers caspase-3-dependent apoptosis in cultured T98G cells

(A) Caspase-3 activation (green) correlating with condensed nuclei (blue) (*upper panels*), overt nuclear condensation (*middle panels*), and plasma membrane blebbing (*lower panels*) after treatment with ST-11 (10 μM) at the indicated times. Scale bars: *upper and middle panels*, 50 μm and 10 μm (*inset*); *lower panels*, 200 μm and 50 μm (*inset*). (B-C) Representative western blots showing activation of caspase-3 24 hrs after ST-11 treatment (3 μM) (B) and an increase in cleaved PARP (C, left) after ST-11 treatment (3 μM) for the indicated times. PARP cleavage was quantified using GAPDH as a loading control (C, right). (D) The antineoplastic effect of ST-11 (10 μM) was ablated by a caspase-3 inhibitor (Z-DEVD-FMK, 10 μM, 15 min preincubation). ***P<0.001 compared with vehicle, one-way ANOVA with Tukey *post-hoc* test. Data are the mean ± SEM of at least 3 independent experiments. (E) Cell number over a 72 hr period measured with WST-1 after treatment with ST-11 (10 μM), nocodazole (10 μM), or paclitaxel (10 μM). ***P<0.001 compared with paclitaxel, ‡p<0.001 compared with nocodazole, two-way ANOVA with Bonferroni *post-hoc* test. Data are the mean ± SEM of at least 3 independent experiments.

Figure 5: LC-MS and pharmacokinetic analysis of ST-11 in mouse serum and brain

(A) Elution time of ST-11 and JWH-015 showing total current (black line) and individual currents from ST-11 and JWH-015. (B-C) Resolution of ST-11 (B) and JWH-015 (C) daughter ions. (D) Quantification of ST-11 extracted from serum and brain matrices shows a linear range of detection from 30 fg–1 ng. (E) Time course of ST-11 levels in serum and brain after i.p. injection of 40 mg/kg ST-11. (F) Brain and serum levels of ST-11 60 min after i.p. injection of the indicated doses. Results are presented as the mean ± SEM of 3 independent experiments.

Figure 6: ST-11 activates caspase-3 and reduces GBM tumor burden in a syngeneic mouse model of GBM

(A) Representative image of a BALB/c mouse brain containing a DBT tumor 3 weeks post-implantation and stained with H&E. Scale bar: 500 μm. Additional H&E features are presented in Figure S1. (B) Daily i.p. treatments of ST-11 for 2 weeks dose-dependently decreased tumor volume *$p<0.05$, one-way ANOVA with Dunnett's *post-hoc* test. Results are mean ± SEM of at least 5 mice. (C) Representative images of activated caspase-3 (red) and DAPI (blue) staining in DBT tumor slices obtained from mice given the indicated treatments. Scale bars: 25 μm and 10 μm (*inset*). Arrows show DBT cells with high levels of activated caspase-3 neighboring condensed nuclei.

Figure 1

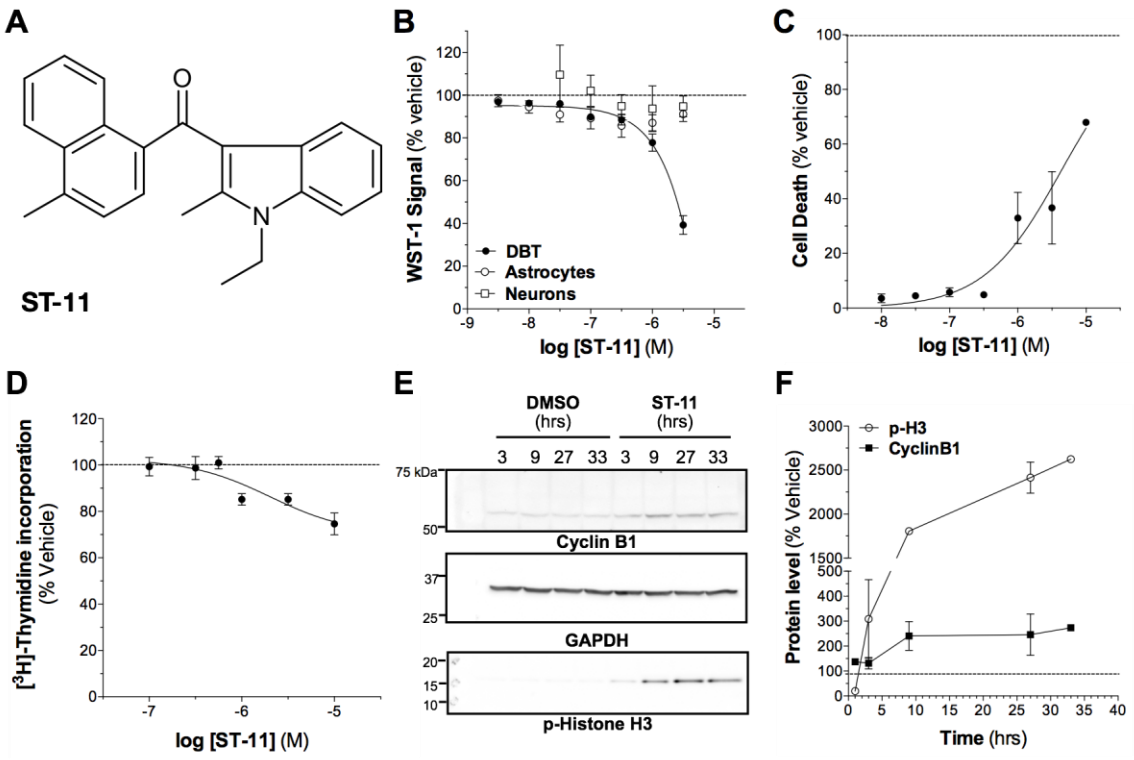
A
O
N
ST-11
B
WST-1 Signal (% vehicle)
DBT
Astrocytes
Neurons
log [ST-11] (M)
C
Cell Death (% vehicle)
log [ST-11] (M)
D
[3H]-Thymidine incorporation (% Vehicle)
log [ST-11] (M)
E
DMSO (hrs)
ST-11 (hrs)
3 9 27 33 3 9 27 33
75 kDa
50
Cyclin B1
37
25
GAPDH
20
15
10
p-Histone H3
F
p-H3
CyclinB1
Protein level (% Vehicle)
Time (hrs)

Figure 2

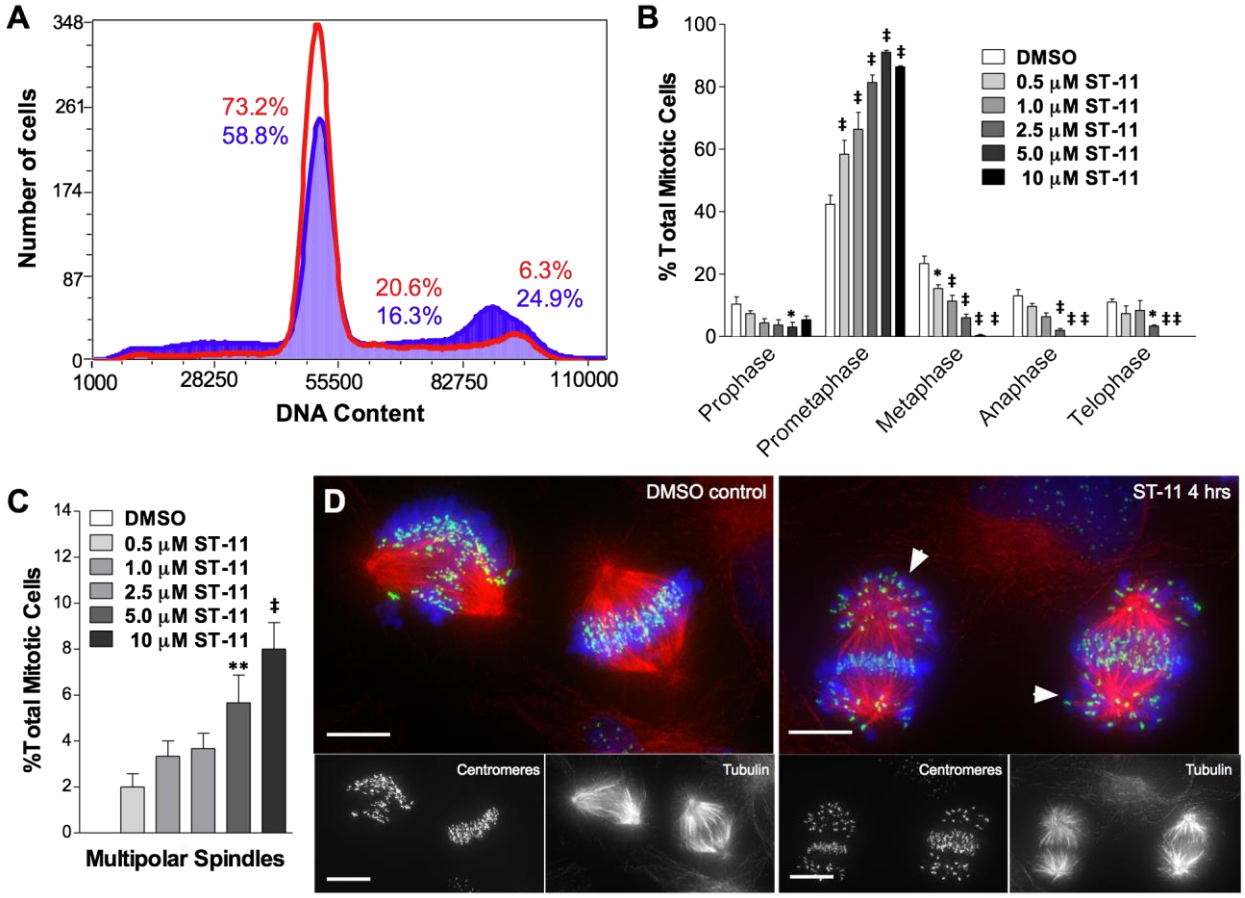
A
Number of cells
348
261
174
87
0
73.2%
58.8%
20.6%
16.3%
6.3%
24.9%
1000
28250
55500
82750
110000
DNA Content
B
% Total Mitotic Cells
100
80
60
40
20
0
DMSO
0.5 μM ST-11
1.0 μM ST-11
2.5 μM ST-11
5.0 μM ST-11
10 μM ST-11
Prophase
Prometaphase
Metaphase
Anaphase
Telophase
C
%Total Mitotic Cells
14
12
10
8
6
4
2
0
DMSO
0.5 μM ST-11
1.0 μM ST-11
2.5 μM ST-11
5.0 μM ST-11
10 μM ST-11
Multipolar Spindles
D
DMSO control
ST-11 4 hrs
Centromeres
Tubulin
Centromeres
Tubulin

Figure 3

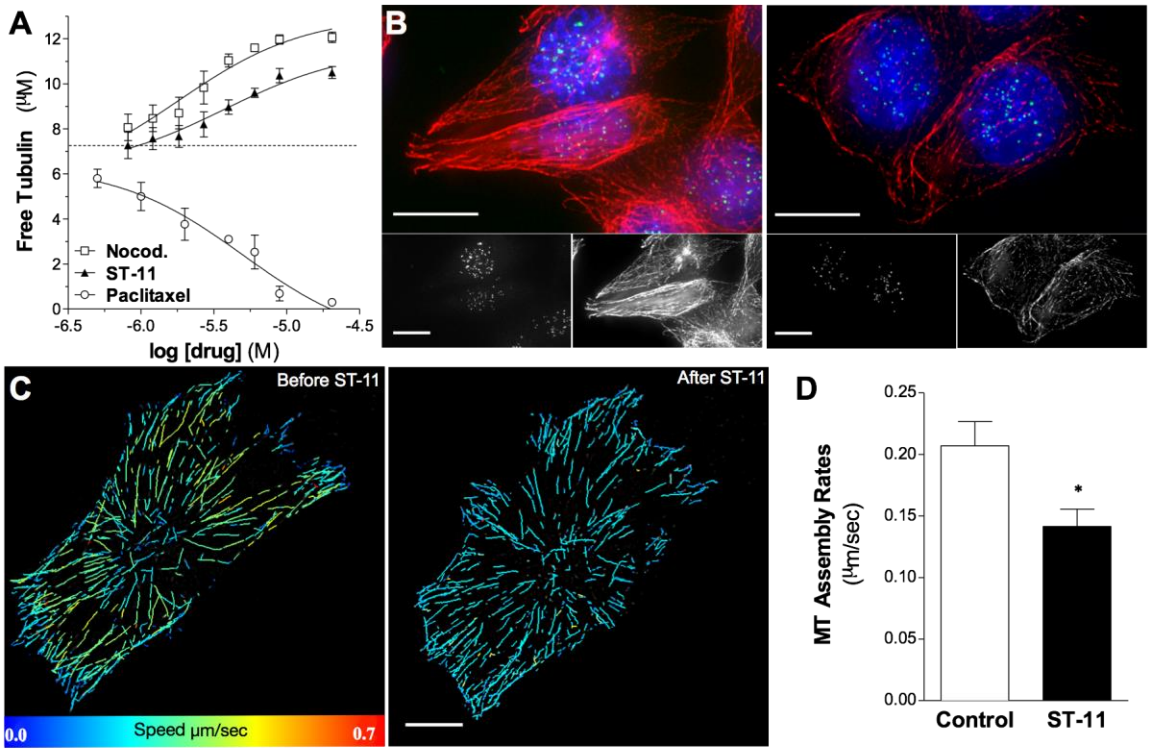
A
Free Tubulin (μM)
12
10
8
6
4
2
0
-6.5
-6.0
-5.5
-5.0
-4.5
log [drug] (M)
Nocod.
ST-11
Paclitaxel
B
C
Before ST-11
After ST-11
0.0
Speed μm/sec
0.7
D
MT Assembly Rates
(μm/sec)
0.25
0.20
0.15
0.10
0.05
0.00
*
Control
ST-11

Figure 4

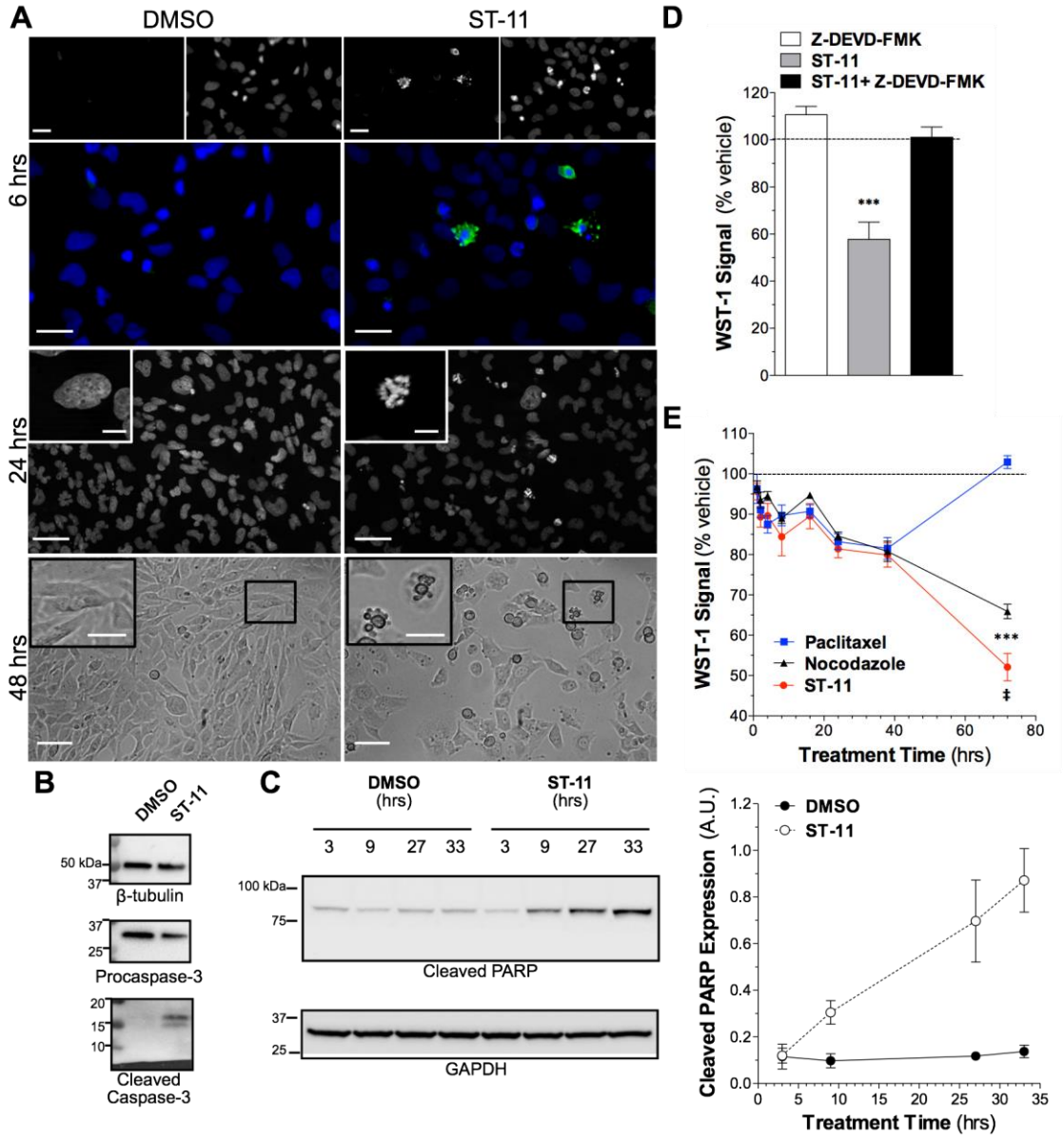
A
DMSO
ST-11
6 hrs
24 hrs
48 hrs
B
DMSO
ST-11
50 kDa
37
β-tubulin
37
25
Procaspase-3
20
15
10
Cleaved Caspase-3
C
DMSO (hrs)
ST-11 (hrs)
3 9 27 33 3 9 27 33
100 kDa
75
Cleaved PARP
37
25
GAPDH
D
Z-DEVD-FMK
ST-11
ST-11+ Z-DEVD-FMK
WST-1 Signal (% vehicle)
120
100
80
60
40
20
0
***
E
WST-1 Signal (% vehicle)
110
100
90
80
70
60
50
40
Paclitaxel
Nocodazole
ST-11
***
‡
0 20 40 60 80
Treatment Time (hrs)
Cleaved PARP Expression (A.U.)
DMSO
ST-11
1.2
1.0
0.8
0.6
0.4
0.2
0.0
0 5 10 15 20 25 30 35
Treatment Time (hrs)

Figure 5

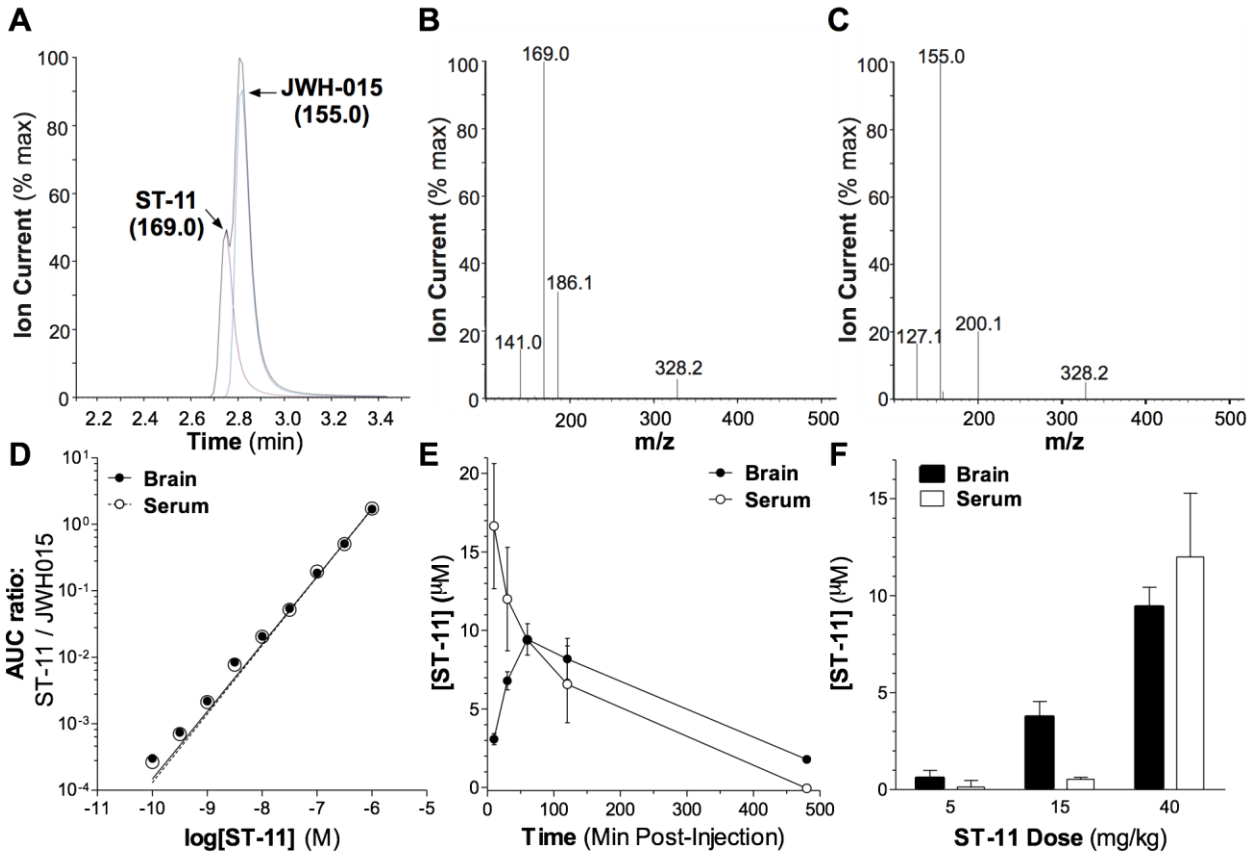
A
B
C
Ion Current (% max)
JWH-015
(155.0)
ST-11
(169.0)
Time (min)
169.0
186.1
141.0
328.2
m/z
155.0
127.1
200.1
328.2
m/z
D
E
F
Brain
Serum
AUC ratio:
ST-11 / JWH015
log[ST-11] (M)
[ST-11] (μM)
Time (Min Post-Injection)
[ST-11] (μM)
ST-11 Dose (mg/kg)

Figure 6

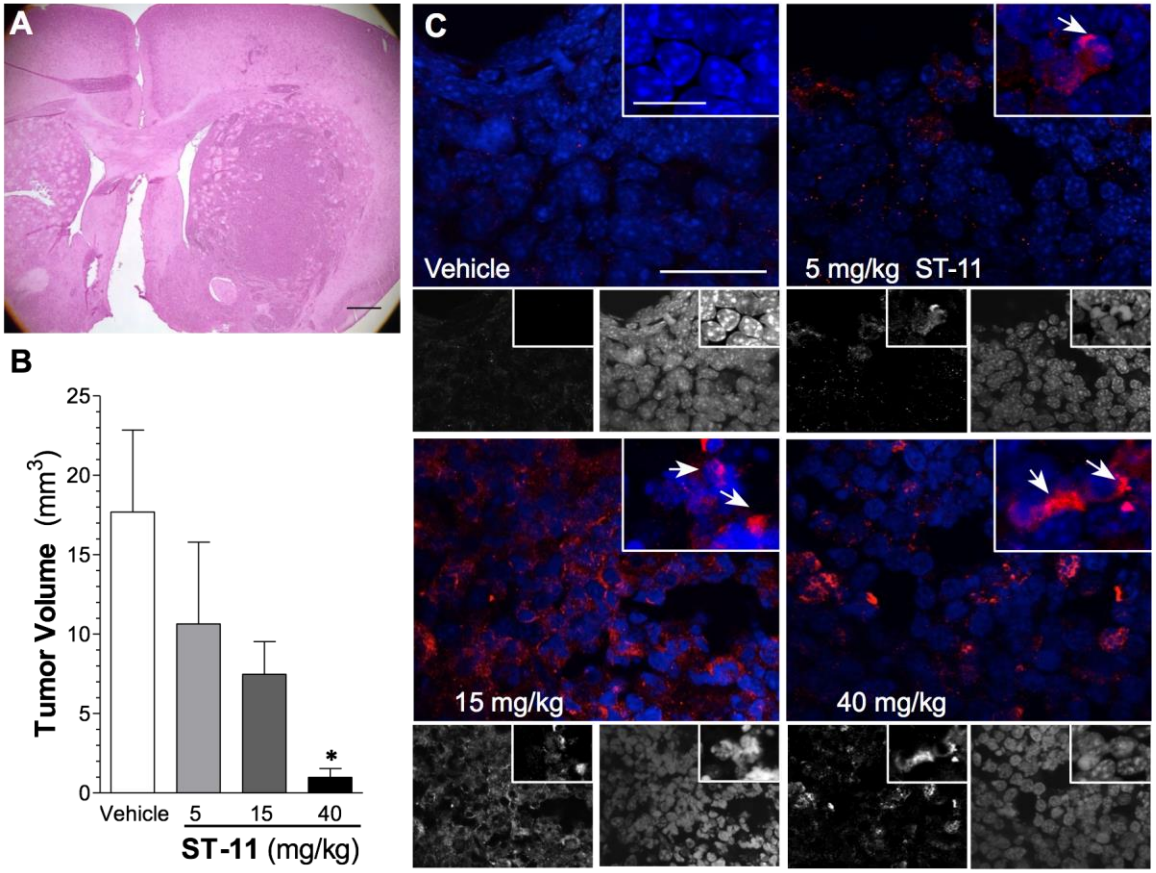
A
B
Tumor Volume (mm3)
25
20
15
10
5
0
*
Vehicle
5
15
40
ST-11 (mg/kg)
C
Vehicle
5 mg/kg ST-11
15 mg/kg
40 mg/kg